Direct Ab Initio Dynamics Studies of the Reaction Paths and Rate Constants of Hydrogen Atom with Germane and Silane

Xin Yu,* Shen-Min Li, Ze-Sheng Li, and Chia-Chung Sun

Institute of Theoretical Chemistry, State Key Laboratory of Theoretical and Computational Chemistry, Jilin University, Changchun 130023, People's Republic of China

Received: February 3, 2000; In Final Form: May 22, 2000

The hydrogen abstraction reactions of hydrogen atom with germane and silane have been studied by using ab initio molecular orbital theory and the canonical variational transition state theory. The potential energy surface information is calculated at the UQCISD/6-311+G** level of theory. Energies along the minimum energy paths are improved by a series of single-point G2//QCISD calculations. The changes of the geometries, generalized normal-mode vibratioanal frequencies, and total curvatures along the reaction paths are discussed. The reaction thermal rate constants for the temperature range 200−1600 K are obtained by canonical variational transition state theory with small-curvature tunneling correction. The calculated results show that the variational effect is small and in the lower temperature range, the small curvature effect is important for the two reactions. Good agreement with experimental values is found for the rate constants over the measured temperature ranges. The rate constants can be fitted to the three-parameter expressions through the whole temperature range 200−1600 K: $k(GeH_4 + H) = 2.0 \times 10^7\ T^{2.12} \exp(-492/T)$ cm^3 mol^{-1} s^{-1}; $k(SiH_4 + H) = 2.27 \times 10^5\ T^{2.69} \exp(-779/T)$ cm^3 mol^{-1} s^{-1}.

Introduction

The reactions of H atom with GeH_4 and SiH_4,

$$GeH_4 + H \rightarrow GeH_3 + H_2 \quad (1)$$

$$SiH_4 + H \rightarrow SiH_3 + H_2 \quad (2)$$

are considered to play a significant part in the chemical vapor deposition (CVD) processes used in the semiconductor industry.[1−5] Reaction 1 is also considered to be one of the processes which determine the abundance of GeH_4 in the atmospheres of Jupiter and Saturn.[6,7] Therefore, reliable rate constants for the two reactions are needed to throw light on the mechanics of CVD processes and on the evolution of planetary atmospheres. Four experimental investigations[8−11] have been reported on the rate constants of reaction 1. The early two studies performed by Choo et al.[8] and Austin et al.[9] produced conflicting results. To resolve the difference and adjudicate between them, Nava et al.[10] and Arthur et al.[11] studied this reaction successively, and they obtained satisfactory agreements. Arthur and cooperators[11] measured rate constants in the temperature range 293−473 K, and combined their results with those of Nava et al.[10] to give a best value for the rate constants over the temperature range 200−500 K of $k = (1.21 \pm 0.10) \times 10^{-10} \exp[(-1008 \pm 25)/T]$ cm^3 s^{-1}. Theoretically, only Arthur and cooperators[11] carried out BEBO (bond energy and bond order method) calculation on this reaction, while at the semiempirical theory level they did not obtain satisfactory results. Their calculated activation energies were substantially higher than the corresponding experimental values. To our knowledge, little theoretical attention has been paid to this reaction.

On the other hand, many investigations[12−25] have been reported on the rate constants of reaction 2 in experiments. But only two of the most recent studies, by Arthur et al.[21] and Goumri et al.,[25] investigated the temperature dependence of k. They gave the rate constants in the temperature ranges 294−487 K and 290−660 K to be $k = (2.3 \pm 0.3) \times 10^{-11} \exp[(-11.6 \pm 0.3 \text{ kJ mol}^{-1})/RT]$ cm^3 s^{-1} and $k = (1.78 \pm 0.11) \times 10^{-10} \exp[-(16.0 \pm 0.2) \text{ kJ mol}^{-1}/RT]$ cm^3 s^{-1}, respectively. Theoretically, to our knowledge, only three studies have been reported on this reaction. Gordon et al.[26] and Tachibana et al.[27] studied the stationary points on the reaction path. As both of their geometry optimizations are based on Hartree−Fock level of theory excluding correlation correction, therefore they did not obtain satisfactory reaction barrier and reaction enthalpy. Goumri et al.[25] made a further study on the reaction kinetics. They calculated the reaction rate constants using the nonvariational transition state theory with Wigner tunneling correction. Basing on MP2/6-31G* optimized geometries and the G2 energy correction, the reaction enthalpy is in agreement with the experimental value. However, due to the limits of method, the calculated imaginary frequency of transition state (TS) is too large, which will narrow the potential barrier and overestimate the tunneling correction.

Our objective in embarking on the present work is to make a systematic theoretical survey of the two hydrogen abstraction reactions. The direct dynamic methods[28] are applied to calculate the reaction rate constants over a wide temperature range from 200 to 1600 K. Direct dynamic methods use electronic structure information, including geometries, energies, gradients, and force constants (Hessian) at selected points on the reaction path to calculate rate constants without the intermediate stage of constructing a full analytical potential energy surface. The present studies are carried out in two stages: In the first stage, ab initio calculations are performed for stationary points and for some extra points along the minimum energy paths (MEP) to obtain potential energy information. In the second stage, the potential energy information is input into the POLYRATE

* Author to whom correspondence should be addressed.

10.1021/jp0004314 CCC: $19.00
Published on Web 09/14/2000

TABLE 1: Geometrical Parameters (distances in angstroms and angles in degrees) of the Equilibrium and Transition-State Structures for the Two Reactions at the UQCISD/6-311+G Level**

	geometrical parameters	this work	exptl[a]
H_2	r_{HH}	0.7436	0.7414
GeH_4 (Td)	r_{GeH}	1.5358	1.5251
GeH_3 (C_{3v})	r_{GeH}	1.5391	
	∠HGeH	110.9819	
$GeH_3-H'-H''$ (C_{3v})	$r_{H'H''}$	1.2551	
	$r_{GeH'}$	1.6153	
	r_{GeH}	1.5359	
	∠H"H′Ge	90.	
	∠HGeH′	108.7979	
SiH_4 (Td)	r_{SiH}	1.4766	1.4798
SiH_3 (C_{3v})	r_{SiH}	1.4777	
	∠HSiH	111.2471	
$SiH_3-H'-H''$ (C_{3v})	$r_{H'H''}$	1.1275	
	$r_{SiH'}$	1.6008	
	r_{SiH}	1.477	
	∠H"H′Si	90.	
	∠HSiH′	108.6207	

[a] Taken from ref 35.

8.4.1[29] to calculate variational transition state theory (VTST) rate constant and its temperature dependence.

Calculation Methods

By means of the GAUSSIAN 98 program,[30] high-level ab initio calculations are carried out for the two reactions. The optimized geometries and frequencies of the stationary points (reactant, transition state, and products) are calculated at the UQCISD/6-311+G** level. At the same level, the minimum energy paths are calculated with a gradient step size of 0.05 $(amu)^{1/2}$ bohr in mass-weighed Cartesian coordinates, and the harmonic vibrational frequencies as well as the force-constant matrixes at the selected points near the transition state are obtained. Because the shape of the MEP is important for the calculation of rate constants, the energies of the MEP are refined by the G2//QCISD method,[31] which applies the G2 method[32] at the UQCISD stationary point geometries and along the UQCISD reaction path.

Canonical variational transition state theory (CVT) is based on the idea of varying the dividing surface along a reference path to minimize the rate constant. In this paper, the POLYRATE 8.4.1 program is performed to obtain the theoretical rate constants using the CVT plus a small-curvature tunneling (SCT) correction method proposed by Truhlar and co-workers.[33,34] The rate constants are calculated at 20 temperatures using mass-scaled Cartesian coordinate. The Euler single-step integrator with a step size of 0.0001 $(amu)^{1/2}$ bohr is used to follow the MEP, and the generalized normal-mode analysis is performed every 0.01 $(amu)^{1/2}$ bohr. The curvature components are calculated using a quadratic fit to obtain the derivative of the gradient with respect to the reaction coordinate.

Results and Discussion

A. Stationary Points. Table 1 lists the geometrical parameters of the equilibrium and transition-state structures of the two reactions at the UQCISD/6-311+G** level along with the available experimental data.[35] It is easy to see that for the two reactions the optimized geometrical parameters of the reactants and products are in good agreement with the experimental data. From these results, it might be inferred that the same accuracy could be expected for calculated transition-state geometries. Both of the reactions have C_{3v} transition states, and the transition states are confirmed with normal-mode analysis to have only one imaginary frequency. Besides, the spin contamination is not severe since the expectation values of S^2 (where S denotes electron spin angular momentum) for the two transition states are 0.7689 and 0.7726 (the true value for the doublet state is 0.75), respectively. In the transition-state structures, the length of bonds Ge−H′ and Si−H′ which will be broken increase by 5% and 8% with respect to the equilibrium bond length of GeH_4 and SiH_4, respectively. The length of the H′−H" bonds that will form hydrogen molecule is 1.7 and 1.5 times, respectively, as large as the equilibrium bond length of the hydrogen molecule. Therefore, both of the transition-state structures are reactant-like, and the reactions will proceed via early transition states. This is the expected behavior from Hammond's postulate, since both of the reactions are exothermic. In addition, the $GeH_4 + H \rightarrow GeH_3 + H_2$ reaction will proceed via an "earlier" transition state in comparison with the reaction of $SiH_4 + H \rightarrow SiH_3 + H_2$.

TABLE 2: Vibrational Frequencies (cm^{-1}) of the Equilibrium and Transition-State Structures for the Two Reactions at the UQCISD/6-311+G Level**

	this work	exptl[a]
H_2	(Σ_g^+) 4419	(Σ_g^+) 4403
GeH_4	(*T2*)835, (*E*)925, (*T2*)2181, (*A1*)2190	(*T2*)819, (*E*)931, (*T2*)2114, (*A1*)2106
GeH_3	(*A1*)713, (*E*)859, (*A1*)2138,(*E*)2163	
$GeH_3-H'-H''$	(*E*)270, (*A1*)802, (*E*)855, (*E*)927, (*A1*)1254, (*A1*)2177, (*E*)2181, (*A1*)1159*i*	
SiH_4	(*T2*)960, (*E*)996, (*A1*)2299, (*T2*)2303	*(T2)*914, *(E)*975, (*A1*)2187, (*T2*)2191
SiH_3	(*A1*)806, (*E*)962, (*A1*)2266, (*E*)2298	
$SiH_3-H'-H''$	(*E*)312, (*A1*)907, (*E*)968, (*E*)1006, (*A1*)1150, (*A1*)2286, (*E*)2302, (*A1*)1398*i*	

[a] Taken from ref 35

The harmonic vibrational frequencies of the equilibrium and transition-state structures of the two reactions at the UQCISD/6-311+G** level are listed in Table 2 along with the available experimental data.[35] It can be seen that most of the calculated frequencies of the reactants and products are slightly greater than that of the available experimental values, and the maximum error between them is about 5%. For the $SiH_4 + H \rightarrow SiH_3 + H_2$ reaction, the calculated imaginary frequency of TS, 1398*i*, is close to the value, 1463*i*, recommended by Goumri et al.[25] of estimated G2 level. They thought the value of 1880*i* calculated at the MP2/6-31G* level is too large, which will narrow the potential barrier and overestimate the tunneling correction. So it is apparent that here the UQCISD method is essential.

Table 3 lists the reaction enthalpies and potential barriers for the two reactions. For $GeH_4 + H \rightarrow GeH_3 + H_2$ reaction, the reaction enthalpies at 298 K obtained by G2//QCISD and UQCISD(ZPE) (UQCISD with ZPE correction) methods are −19.22 and −19.17 kcal/mol, respectively. For $SiH_4 + H \rightarrow SiH_3 + H_2$ reaction, they are −12.58 and −12.43 kcal/mol, respectively. Obviously there is a minor difference in the reaction enthalpy between G2//QCISD and UQCISD(ZPE) methods, and they are both close to the corresponding experimental values −20.82 and −12.39 kcal/mol derived from the experimental standard heats of formation (GeH_4, 21.71 kcal/mol;[35] H, 52.12 kcal/mol;[35] GeH_3, 53 kcal/mol;[36] H_2, 0.0 kcal/

TABLE 3: Reaction Enthalpies (ΔH^0_{298}) and Potential Barriers (ΔE) (kcal/mol) for the Two Reactions[a]

		G2//QCISD	UQCISD (ZPE)	exptl
$GeH_4 + H \rightarrow GeH_3 + H_2$	ΔH^0_{298}	−19.22	−19.17	−20.82
	ΔE	3.54	4.60	
$SiH_4 + H \rightarrow SiH_3 + H_2$	ΔH^0_{298}	−12.58	−12.43	−12.39
	ΔE	5.54	6.42	

[a] Total energies (in hartrees); For $GeH_4 + H \rightarrow GeH_3 + H_2$, at UQCISD(ZPE): GeH_4, −2077.751527; H, −0.499810; GeH_3, −2077.124480; H_2, −1.158274; TS, −2078.244009. At G2//QCISD: GeH_4, −2077.797906; H, −0.50; GeH_3, −2077.163183; H_2, −1.166254; TS, −2078.292265. For $SiH_4 + H \rightarrow SiH_3 + H_2$, at UQCISD(ZPE): SiH_4, −291.369023; H, −0.499810; SiH_3, −290.731266; H_2, −1.158274; TS, −291.858597. At G2//QCISD: SiH_4, −291.418468; H, −0.50; SiH_3, −290.773151; H_2, −1.166254; TS, −291.909644.

mol; SiH_4, 8.20 kcal/mol;[37] SiH_3, 47.93 kcal/mol;[38]). Table 3 also shows the reaction potential barriers for the two reactions. For $GeH_4 + H \rightarrow GeH_3 + H_2$ reaction, the potential barriers obtained by G2//QCISD and UQCISD(ZPE) methods take the values 3.54 and 4.60 kcal/mol, respectively. For $SiH_4 + H \rightarrow SiH_3 + H_2$ reaction, they are 5.54 and 6.42 kcal/mol, respectively. Obviously, the G2//QCISD method decreases the reaction potential barriers by about 1 kcal/mol. Therefore, the G2//QCISD method applied here is essential to improve the potential energy curve.

B. Reaction Path Properties. The minimum energy paths (MEP) of the two reactions are calculated at the UQCISD/6-311+G** level by the intrinsic reaction coordinate theory from the transition state to the reactants and products, respectively. The energies of MEP are refined by G2//QCISD method, and for both reactions the maximum for the $V_{MEP}(s)$ is shifted toward the reactants to approximately $s = -0.05$ (amu)$^{1/2}$ bohr. This kind of shifting is artificially caused by the computational technique, which consists of optimizing geometries at a lower level A (here A is UQCISD) and then calculating the energies (without re-optimization) at a higher level B (here B is G2//QCISD). In POLYRATE 8.4.1, the RODS (reorient the dividing surface) algorithm can be used to reorient the generalized transition-state theory dividing surface. Thus the conceptual mistake of taking as a variational effect what is only a numerical defect is avoided. Figure la,b shows the changes of bond lengths along MEP as functions of s (amu)$^{1/2}$ bohr. For both of the reactions, the changes are very similar. First, the breaking bonds (Ge−H′ and Si−H′) and the forming bond (H′−H") change strongly, while the other bonds keep no change. Second, the Ge−H′ and Si−H′ bond distances remain insensitive up to $s = -0.5$ (amu)$^{1/2}$ bohr, and then increase smoothly. While the H′−H" distances rapidly shorten from reactants and arrive to the equilibrium bond length of hydrogen molecule at about $s = 0.75$ and 0.5 (amu)$^{1/2}$ bohr, respectively. A likely explanation for the difference emerges from a consideration of the different transition-state structures. In GeH_3−H′−H" structure, the distance of H′−H" (1.2551 Å) is larger than that of H′−H" (1.1275 Å) in SiH_3−H′−H" structure.

Figure 2a,b depicts the classical potential energy, V_{MEP}, the ground-state vibrational adiabatic potential energy, V_a^G, and the zero-point energy for the two reactions as functions of s (amu)$^{1/2}$ bohr at the G2//QCISD level. For both reactions, the maximum position of the $V_{MEP}(s)$ and $V_a^G(s)$ energy curves is the same, and the zero-point energy curve is practically constant as s varies with only a gentle fall near the saddle point ($s = 0$). To analyze this behavior in greater detail, we show the variations of the generalized normal mode vibrational frequencies along the MEP in Figure 3a,b.

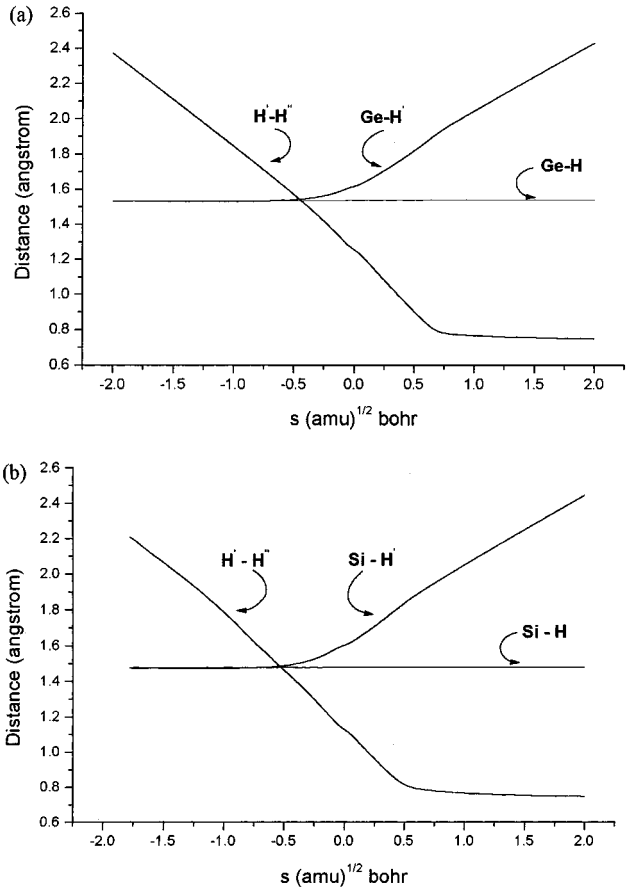

Figure 1. (a) Changes of the main bond lengths (in angstroms) for the $GeH_4 + H \rightarrow GeH_3 + H_2$ reaction as functions of s (amu)$^{1/2}$ bohr at the UQCISD/6-311+G** level. (b) Same as those in (a) except for the $SiH_4 + H \rightarrow SiH_3 + H_2$ reaction.

In the negative limit of s, the frequencies are associated with the reactants $GeH_4 + H$ and $SiH_4 + H$, respectively. In the positive limit of s, the frequencies are associated with the products $GeH_3 + H_2$ and $SiH_3 + H_2$, respectively. In the vicinity of the transition state, there are eleven vibrational frequencies. The harmonic vibrational frequencies of the Ge−H′ and Si−H′ stretches, corresponding to the generalized normal mode breaking during the reactions, drop dramatically near the saddle point. These behaviors are known as typical of hydrogen transfer reactions. [39] A priori, these drops should cause considerable falls in the zero-point energy near the saddle point. The two lowest harmonic frequencies corresponding to free rotations and translations of the reactants evolve to vibrations at about $s = -0.25$ (amu)$^{1/2}$ bohr, and they present a maximum near the saddle point. The behaviors of these two lowest frequencies compensate the falls in the zero-point energy caused by the Ge−H′ and Si−H′ stretches, respectively. As a result, the zero-point energies show very little change with s (Figure 2a,b), and the classical potential energy (V_{MEP}) and the vibrationally adiabatic ground-state potential energy (V_a^G) curves are similar in shape. This analysis indicates that, for the two reactions, the variational effect will be small or almost negligible.

Figure 4a,b shows the changes of the total reaction-path curvature for the two reactions as functions of s (amu)$^{1/2}$ bohr at the G2//QCISD level. There are two sharp peaks for both reactions, one before and one after the saddle point. For the reaction of $GeH_4 + H \rightarrow GeH_3 + H_2$, the positions of the peaks are at $s = -0.2$ and 0.6 (amu)$^{1/2}$ bohr, due to the strong couplings of the reaction coordinate with the Ge−H′, and H'−H" stretches, respectively. For the reaction of $SiH_4 + H \rightarrow SiH_3$

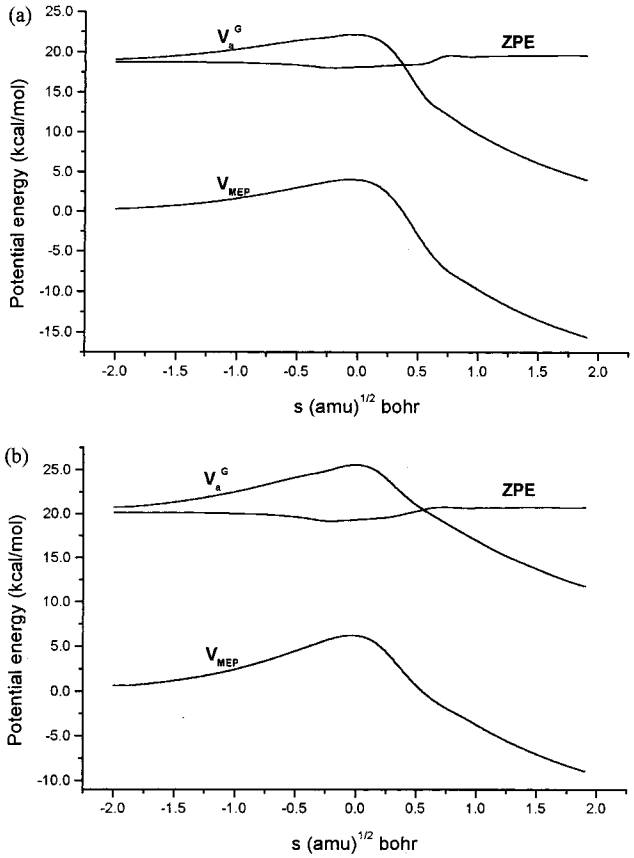

Figure 2. (a) Classical potential energy (V_{MEP}), ground-state vibrationally adiabatic potential energy (V_a^G), and zero-point energy (ZPE) for the $GeH_4 + H \rightarrow GeH_3 + H_2$ reaction as functions of s (amu)$^{1/2}$ bohr at the G2//QCISD level. (b) Same as those in (a) except for the $SiH_4 + H \rightarrow SiH_3 + H_2$ reaction.

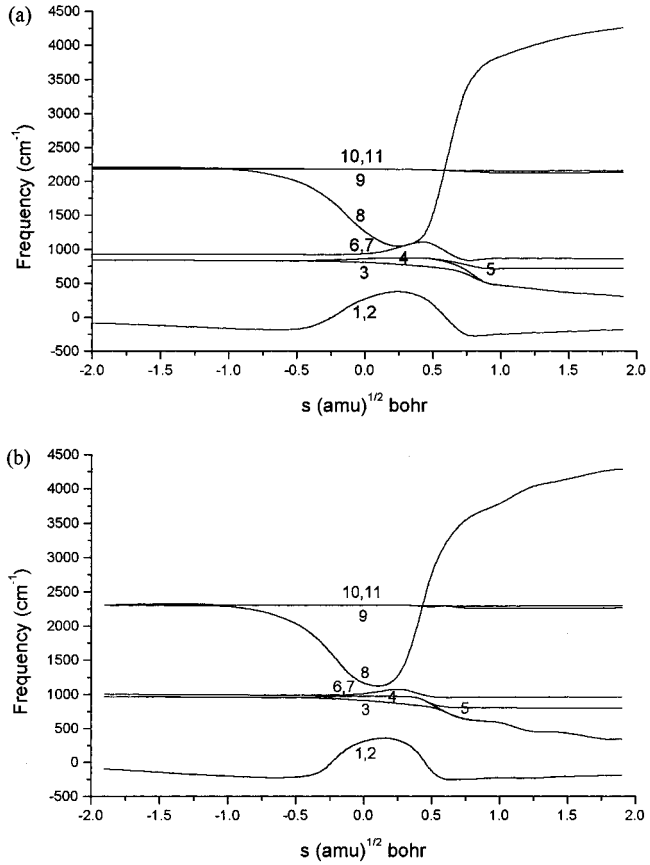

Figure 3. (a) Changes of the generalized normal-mode vibrational frequencies for the $GeH_4 + H \rightarrow GeH_3 + H_2$ reaction as functions of s (amu)$^{1/2}$ bohr at the UQCISD/6-311+G** level. (b) Same as those in (a) except for the $SiH_4 + H \rightarrow SiH_3 + H_2$ reaction.

$+ H_2$, the positions of the peaks are at $s = -0.1$ and 0.4 (amu)$^{1/2}$ bohr, due to the strong couplings of the reaction coordinate with the Si−H′ and H−H′ stretches, respectively. Notice that the reaction path curvatures of the two reactions are not severe, therefore, the small-curvature tunneling correction method for calculating the reaction rate constants should be suitable.

By the analysis of how the bond lengths, potential energies, frequencies, and total curvatures vary as functions of the reaction coordinate, it is easy to see that the changes of the two reactions are very similar. The difference is that the range of the "reaction region" of $GeH_4 + H \rightarrow GeH_3 + H_2$ is slightly larger than that of $SiH_4 + H \rightarrow SiH_3 + H_2$.

Rate Constant Calculation. The canonical variational transition state theory rate constants with a small-curvature tunneling correction for the two reactions are calculated in a wide temperature range from 200 to 1600 K at the G2//QCISD level. Figure 5a,b displays the plots of the calculated results along with the available experimental values for the two reactions. It can be seen that the rate constants of TST (line 1) and CVT (line 2) are nearly the same in the whole temperature range 200−1600 K, which enables us to conclude that the variational effect for the two reactions is very small or almost negligible. Also, in comparison with the rate constants of TST and CVT in the measured temperature ranges, the CVT/SCT rate constants (line 3) are in much better agreement with the corresponding experimental values[7,21,25] for the two reactions. However, in the higher temperature range, the CVT/SCT rate constants (line 3) are asymptotic to the rate constants of TST (line 1) and CVT (line 2), which means only in the lower temperature range the small-curvature tunneling (SCT) correction plays an important role for the two reactions. The same results can be seen clearly from Tables 4 and 5 that list the reaction rate constants for the two reactions in the temperature range 200−1600 K. For example, for $SiH_4 + H \rightarrow SiH_3 + H_2$ reaction, at 290 K the experimental rate constants are 37, 38, and 2.6 times as large as the calculated ones derived from the TST, CVT, and CVT/SCT methods, respectively. While at 658 K, the multiplying factors are 3.8, 4.1, and 2.4, respectively. The rate constants of CVT/SCT at the UQCISD/6-311+G** level are also plotted in Figure 5a,b. They are not in good agreement with the experimental values in comparison with the rate constants of CVT/SCT at the G2//QCISD level for both reactions. Notice that even at the G2//QCISD level, there is a slight discrepancy between the CVT/SCT rate constants and experimental values. We think the calculated potential energy curve is not accurate enough. That is to say even at the present G2//QCISD level, the potential barrier still has been overestimated. On the other hand, the potential barrier is difficult to compare with experiment since it is not measured directly, thus the calculated reaction activation energies are given in order to provide the most possible comparison with the experiments. For $GeH_4 + H \rightarrow GeH_3 + H_2$ reaction, the calculated activation energy in the experimentally measured temperature range 210−473 K are 2.26 and 2.73 kcal/mol, respectively, at the G2//QCISD and UQCISD/6-311+G** level. The former is much closer to the experimental value, 2.00 kcal/mol.[7] For $SiH_4 + H \rightarrow SiH_3 + H_2$ reaction, the calculated activation energies are given in the experimentally measured temperature ranges 294−487 K[21] and 290−660 K[25], and they are 3.56 and 3.88 kcal/mol at the G2//QCISD level

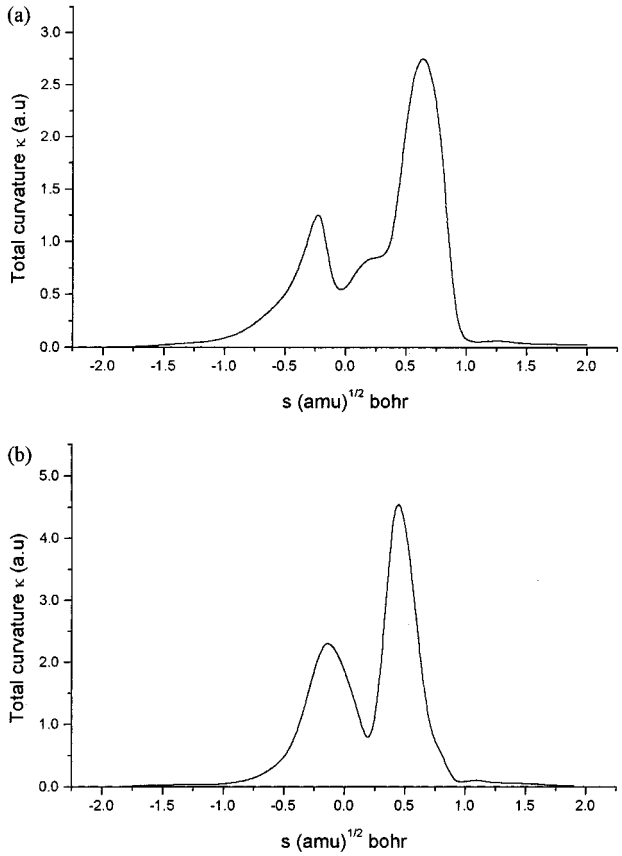

Figure 4. (a) Changes of the total reaction-path curvature for the $GeH_4 + H \rightarrow GeH_3 + H_2$ reaction as functions of s (amu)$^{1/2}$ bohr at the G2//QCISD level. (b) Same as those in (a) except for the $SiH_4 + H \rightarrow SiH_3 + H_2$ reaction.

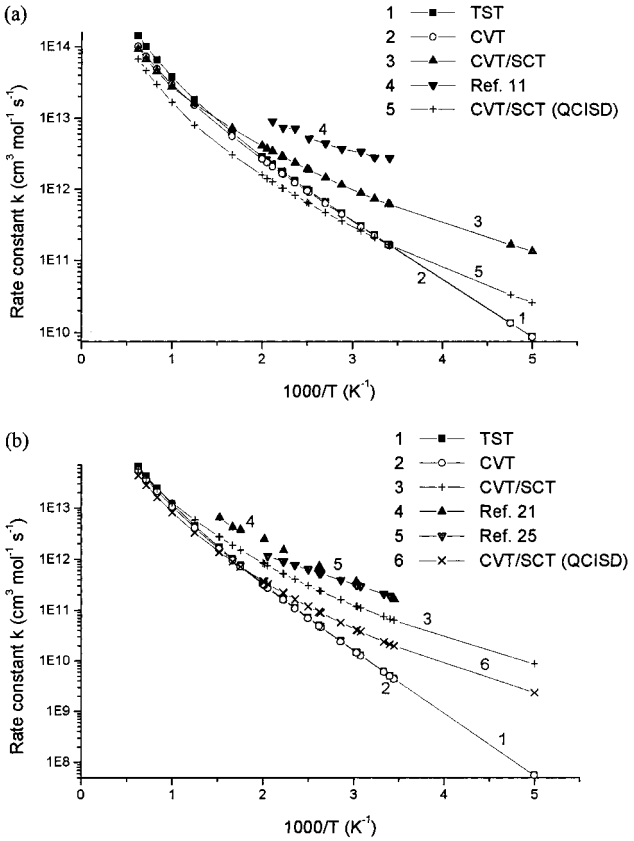

Figure 5. (a) Plot of the calculated rate constants k (cm^3 mol^{-1} s^{-1}) versus 1000/T and available experimental data for the $GeH_4 + H \rightarrow GeH_3 + H_2$ reaction. (b). Same as those in (a) except for the $SiH_4 + H \rightarrow SiH_3 + H_2$ reaction.

with respect to 4.04 and 4.38 kcal/mol at the UQCISD/6-311+G** level, respectively. The values calculated at the G2//QCISD level are much closer to 2.77 and 3.83 kcal/mol obtained by the experiments.[21,25] By comparison between theoretical and experimental rate constants and between theoretical and experimental activation energies, it is not difficult to find that the G2//QCISD method is more reliable than the UQCISD/6-311+G** method for the two reactions. In addition, the reaction rate constants of $GeH_4 + H \rightarrow GeH_3 + H_2$ are about 1 order of magnitude higher in comparison with the rate constants of $SiH_4 + H \rightarrow SiF_3 + H_2$ in the temperature range 294−487 K. This is in accordance with the experimental results.[11,25] Finally, we present three-parameter fits for rate constants of the two reactions in the temperature range 200−1600 K to describe the non-Arrhenius behavior of the rate constants in the broader temperature range. The expressions are $k(GeH_4 + H) = 2.0 \times 10^7\ T^{2.12} \exp(-492/T)$ cm^3 mol^{-1} s^{-1} and $k(SiH_4 + H) = 2.27 \times 10^5\ T^{2.69} \exp(-779/T)$ cm^3 mol^{-1} s^{-1}, respectively.

TABLE 4: Rate Constants (cm^3 mol^{-1} s^{-1}) for the Reaction of $GeH_4 + H \rightarrow GeH_3 + H_2$ in the Temperature Range 200−1600 K at the G2//QCISD Level

T	TST	CVT	CVT/SCT	exptl[a]
200	8.79×10^9	8.73×10^9	1.34×10^{11}	
210	1.36×10^{10}	1.35×10^{10}	1.66×10^{11}	
293	1.64×10^{11}	1.61×10^{11}	6.08×10^{11}	2.74×10^{12}
308	2.25×10^{11}	2.20×10^{11}	7.29×10^{11}	2.78×10^{12}
323	3.02×10^{11}	2.93×10^{11}	8.73×10^{11}	3.32×10^{12}
347	4.59×10^{11}	4.41×10^{11}	1.14×10^{12}	3.68×10^{12}
370	6.57×10^{11}	6.26×10^{11}	1.45×10^{12}	4.37×10^{12}
397	9.52×10^{11}	9.03×10^{11}	1.87×10^{12}	5.17×10^{12}
400	9.94×10^{11}	9.40×10^{11}	1.92×10^{12}	
423	1.31×10^{12}	1.23×10^{12}	2.33×10^{12}	7.16×10^{12}
448	1.74×10^{12}	1.62×10^{12}	2.84×10^{12}	7.34×10^{12}
450	1.78×10^{12}	1.65×10^{12}	2.89×10^{12}	
473	2.24×10^{12}	2.07×10^{12}	3.40×10^{12}	8.97×10^{12}
500	2.88×10^{12}	2.64×10^{12}	4.06×10^{12}	
600	6.20×10^{12}	5.54×10^{12}	7.11×10^{12}	
800	1.80×10^{13}	1.51×10^{13}	1.57×10^{13}	
1000	3.74×10^{13}	2.96×10^{13}	2.73×10^{13}	
1200	6.44×10^{13}	4.87×10^{13}	4.44×10^{13}	
1400	9.94×10^{13}	7.23×10^{13}	6.57×10^{13}	
1600	1.42×10^{14}	1.01×10^{14}	9.15×10^{13}	

[a] Taken from ref 11.

Conclusions

In this paper, the hydrogen abstraction reactions: $GeH_4 + H \rightarrow GeH_3 + H_2$ and $SiH_4 + H \rightarrow SiH_3 + H_2$ have been investigated theoretically. The changes of the bond lengths, potential energies, frequencies, and total curvatures along the reaction path of the two reactions are very similar. The main differences of the two reactions lie in the following three points: (1) At the G2//QCISD level of theory, the potential barrier of $GeH_4 + H \rightarrow GeH_3 + H_2$ reaction is lower than that of $SiH_4 + H \rightarrow SiH_3 + H_2$ by about 2 kcal/mol. So the $GeH_4 + H \rightarrow GeH_3 + H_2$ reaction is easier to proceed. (2) Since the reaction of $GeH_4 + H \rightarrow GeH_3 + H_2$ is more exothermic, it proceeds via an "earlier" transition state. (3) The range of the "reaction region" of $GeH_4 + H \rightarrow GeH_3 + H_2$ is slightly larger than that of $SiH_4 + H \rightarrow SiH_3 + H_2$.

The reaction rate constants in the temperature range 200−1600 K are calculated at the G2//QCISD level by the canonical variational transition state theory (CVT) with the small-curvature tunneling (SCT) correction. The calculation results show that

TABLE 5: Rate Constants ($cm^3\ mol^{-1}\ s^{-1}$) for the Reaction of $SiH_4 + H \rightarrow SiH_3 + H_2$ in the Temperature Range 200−1600 K at the G2//QCISD Level

T	TST	CVT	CVT/SCT	exptl[a]
200	5.55×10^7	5.54×10^7	8.55×10^9	
290	4.37×10^9	4.30×10^9	$6{,}20 \times 10^{10}$	1.63×10^{11}
300	6.08×10^9	5.97×10^9	7.35×10^{10}	
329	1.43×10^{10}	1.40×10^{10}	1.16×10^{11}	3.31×10^{11}
330	1.46×10^{10}	1.43×10^{10}	$1.18 \times l0^{11}$	3.61×10^{11}
350	2.44×10^{10}	2.37×10^{10}	1.57×10^{11}	
379	4.67×10^{10}	4.52×10^{10}	2.31×10^{11}	6.38×10^{11}
382	4.97×10^{10}	4.81×10^{10}	2.40×10^{11}	7.04×10^{11}
400	$7.11 \times l0^{10}$	6.81×10^{10}	2.99×10^{11}	
449	1.64×10^{11}	1.57×10^{11}	5.13×101^{1}	1.47×10^{12}
496	3.18×10^{11}	3.02×10^{11}	8.07×10^{11}	2.40×10^{12}
500	3.35×10^{11}	$3.18 \times l0^{11}$	8.37×10^{11}	
570	7.47×10^{11}	7.05×10^{11}	1.48×10^{12}	3.67×10^{12}
600	1.00×10^{12}	9.40×10^{11}	1.84×10^{12}	4.12×10^{12}
658	1.66×10^{12}	1.54×10^{12}	2.67×10^{12}	6.33×10^{12}
800	4.38×10^{12}	4.01×10^{12}	5.65×10^{12}	
1000	1.17×10^{13}	1.04×10^{13}	1.25×10^{13}	
1200	2.39×10^{13}	2.08×10^{13}	2.32×10^{13}	
1400	4.16×10^{13}	3.57×10^{13}	3.82×10^{13}	
1600	6.50×10^{13}	5.52×10^{13}	5.75×10^{13}	

[a] The value is the larger one at every temperature selected from ref 25.

for the two reactions the reaction activation energies and the CVT/SCT rate constants are in good agreement with the experimental ones in the measured temperature ranges. The variational effect on the values of rate constant is small, and the tunneling correction is important in the calculations of rate constant in the lower temperature range. The three-parameter fits for the two reactions in the temperature range 200−1600 K are $k(GeH_4 + H) = 2.0 \times 10^7\ T^{2.12} \exp(-492/T)\ cm^3\ mol^{-1}\ s^{-1}$ and $k(SiH_4 + H) = 2.27 \times 10^5\ T^{2.69} \exp(-779/T)\ cm^3\ mol^{-1}\ s^{-1}$, respectively.

Acknowledgment. Authors thank Professor Donald G. Truhlar for providing the POLYRATE 8.4.1 program. This work is supported by the National Science Foundation of China.

References and Notes

(1) Doyle, J. R.; Doughty, D. A.; Gallagher, A. *J. Appl. Phys.* **1991**, *69*, 4169.
(2) Kushner, M. J. *J. Appl. Phys.* **1987**, *62*, 2803.
(3) Kushner, M. J. *J. Appl. Phys.* **1988**, *63*, 2532.
(4) Ryan, K. J.; Plumb, I. C. *CRC Crit. Rev. Solid State Mater. Sci.* **1988,** *15*, 153.
(5) Roth, A.; Comes, F. J. *Ber Bunsen-Ges. Phys. Chem.* **1991**, *95*, 1296.
(6) Fegley, B., Jr.; Prinn, R. G. *Astrophys. J.* **1985**, *299*, 1067.
(7) Noll, K. S.; Knacke, R. F.; Geballe, T. R.; Tokunaga, A. T. *Icarus* **1988**, *75*, 409.
(8) Choo, K. Y.; Gaspar, P. P.; Wolf, A. P. *J. Phys. Chem.* **1975**, *79*, 1752.
(9) Austin, E. R.; Lampe, F. W. *J. Phys. Chem.* **1977**, *81*, 1134.
(10) Nava, D. F.; Payne, W. A.; Marston, G.; Stief, L. J. *J. Geophys. Res.* **1993**, *98*, 5331.
(11) Arthur, N. L.; Cooper, I. A. *J. Chem. Soc., Faraday Trans.* **1995**, *91*, 3367.
(12) Niki, H.; Mains, G. J. *J. Phys. Chem.* **1964**, *68*, 304.
(13) Lightfoot, P. D.; Pilling, M. J. *J. Phys. Chem.* **1987**, *91*, 3373.
(14) Moortgat, G. K. Ph.D. Thesis, University of Detroit, 1970.
(15) Hong, J. H. Ph.D. Thesis, University of Detroit, 1972.
(16) Cowfer, J. A.; Lynch, K. P.; Michael, J. V. *J. Phys. Chem.* **1975**, *79*, 1139.
(17) Choo, K. Y.; Gaspar, P. P.; Wolf, A. P. *J. Phys. Chem.* **1975**, *79*, 1752.
(18) Austin, E. A.; Lampe, F. W. *J. Phys. Chem.* **1977**, *81*, 1134.
(19) Mihelcic, D.; Schubert, V.; Schindler, R. N.; Potzinger, P. *J. Phys. Chem.* **1977**, *81*, 1543.
(20) Worsdorfer, K.; Reimann, B.; Potzinger, P. *Z. Naturforsch.* **1983,** *38a*, 896.
(21) Arthur, N. L.; Porzinger, P.; Reimann, B.; Steenbergen, H. P. *J. Chem. Soc., Faraday Trans. 2* **1989**, *85*, 1447.
(22) Koshi, M.; Tamura, F.; Matsui, H. *Chem. Phys. Lett.* **1990**, *173*, 235.
(23) Potzinger. P.; Glasgow, L. C.; Reimann, B. *Z. Naturforsch.* **1974**, *29a*, 493.
(24) Mihelcic, D.; Potzinger, P.; Schindler, R. N. *Ber. Bunsen-Ges. Phys. Chem.* **1976**, *80*, 565.
(25) Goumri, A.; Yuan. W. J.; Ding, L. Y.; Shi, Y. C.; Marshall, P. *Chem. Phys.* **1993,** *177*, 233.
(26) Gordon, M. S.; Gano, D. R.; Boatz, J. A. *J. Am. Chem. Soc.* **1983**, *105* (5), 5771.
(27) Tachibana, A.; Kurosaki, Y.; Yamaguchi, K.; Yamabe, T. *J. Phys. Chem.* **1991**, *95*, 6849.
(28) Truhlar, D. G.; Gordon, M. S. *Science* **1990,** *249*, 491.
(29) Chuang, Y.-Y.; Corchado, J. C.; Fast, P. L.; Villa, J.; Hu, W.-P.; Liu, Y.-P.; Lynch, G. C.; Jackels, C. F.; Nguyen, K. A.; Gu, M. Z.; Rossi, I.; Coitino, E. L.; Clayton, S.; Melissas, V. S.; Lynch, B. J.; Steckler, R.; Garrett, B. C.; Isaacson, A. D.; Truhlar, D. G. *POLYRATE version 8.4.1*, University of Minnesota, Minneapolis, 2000.
(30) Frisch, M. J.; Trucks, G. W.; Schlegel, H. B.; Scuseria, G. E.; Robb, M. A.; Cheeseman, J. R.; Zakrzewski, V. G.; Montgomery, J. A., Jr.; Stratmann, R. E.; Burant, J. C.; Dapprich, S.; Millam, J. M.; Daniels, A. D.; Kudin, K. N.; Strain, M. C.; Farkas, O.; Tomasi, J.; Barone, V.; Cossi, M.; Cammi, R.; Mennucci, B.; Pomelli, C.; Adamo, C.; Clifford, S.; Ochterski, J.; Petersson, G. A.; Ayala, P. Y.; Cui, Q.; Morokuma, K.; Malick, D. K.; Rabuck, A. D.; Raghavachari, K.; Foresman, J. B.; Cioslowski, J.; Ortiz, J. V.; Baboul, A. G.; Stefanov, B. B.; Liu, G.; Liashenko, A.; Piskorz, P.; Komaromi, I.; Gomperts, R.; Martin, R. L.; Fox, D. J.; Keith, T.; Al-Laham, M. A.; Peng, C. Y.; Nanayakkara, A.; Gonzalez, C.; Challacombe, M.; Gill, P. M. W.; Johnson, B.; Chen, W.; Wong, M. W.; Andres, J. L.; Gonzalez, C.; Head-Gordon, M.; Replogle, E. S.; Pople, J. A. *GAUSSIAN 98*; Gaussian, Inc.: Pittsburgh, PA, 1998.
(31) Durant, J. L., Jr.; Rohlfing, C. M. *J. Chem. Phys.* **1993,** *98*, 8031.
(32) Curtiss, L. A.; Raghavachari, L.; Trucks, G. W.; Pople, J. A. *J. Chem. Phys.* **1991,** *94*, 7221.
(33) Truhlar, D. G.; Isaacson, A. D.; Garret, B. C. In *Theory of Chemical Reaction Dynamics*; Baer, M., Ed.; CRC Press: Boca Raton, FL, 1985; p 65.
(34) Steckler, R.; Hu, W.-P.; Liu, Y.-P.; Lynch, G. C.; Garrett, B. C.; Isaacson, A. D.; Melissas, V. S.; Lu, D.-H.; Troung, T. N.; Rai, S. N.; Hancock, G. C.; Lauderdale, J. G.; Joseph, T.; Truhlar, D. G. *Comput. Phys. Commun.* **1995**, *88*, 341.
(35) Lide, D. R. In *CRC Handbook of Chemistry and Physics*, 79th ed.; CRC Press: NewYork, 1998.
(36) Berkowitz, J.; Ellison, G. B.; Gutman, D. *J. Phys. Chem.* **1994**, *98*, 2744.
(37) Chase, M. W., Jr. *J. Phys. Chem.* Ref. Data, Monograph 9, **1998,** pp 1−1951.
(38) Seetula, J. A.; Feng, Y.; Gutman, D.; Seakins, P. W.; Pilling, M. J. *J. Phys. Chem.* **1991**, *95*, 1658.
(39) Kraka, E.; Dunning, T. H. Jr. In *Advances in Molecular Electronic Structure Theory;* Dunning, T. H. Jr., Ed.; JAI press: Greenwich, 1990; Vol. I.